iScience

Article

Distinct eccentricity-driven dynamics in foveal and extrafoveal visual crowding

Graphical abstract

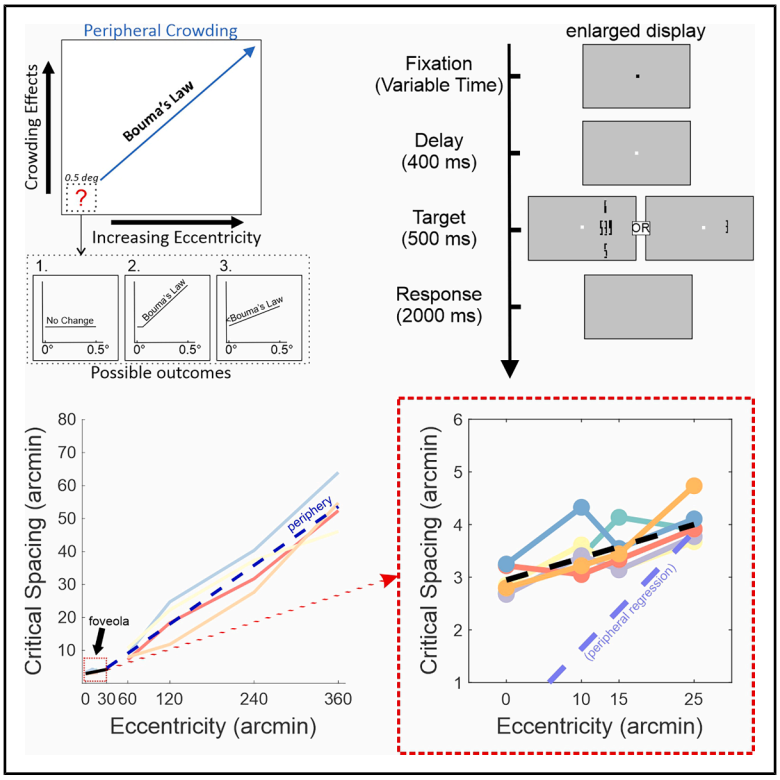

Highlights

- With high-precision eye tracking, crowding was measured across the central 0.5°
- Unflanked acuity and edge-to-edge crowding thresholds diverged with eccentricity
- Foveolar crowding increased with eccentricity ~3.5× slower than extrafoveally
- Peripheral unflanked acuity matched midget RGC spacing, unlike crowding thresholds

Authors

Ashley M. Clark,
Krishnamachari S. Prahalad,
Martina Poletti

Correspondence

martina_poletti@urmc.rochester.edu

In brief

Ophthalmology; Neuroscience

Clark et al., 2026, iScience 29, 115168
April 17, 2026
https://doi.org/10.1016/j.isci.2026.115168

CellPress

iScience

CellPress
OPEN ACCESS

Article

Distinct eccentricity-driven dynamics in foveal and extrafoveal visual crowding

Ashley M. Clark,[1,2,4] Krishnamachari S. Prahalad,[1,2,4] and Martina Poletti[1,2,3,5,*]
[1]Department of Brain and Cognitive Sciences, University of Rochester, Meliora Hall, Rochester, NY 14627, USA
[2]Center for Visual Science, University of Rochester, 361 Meliora Hall, Rochester, NY 14627, USA
[3]Department of Neuroscience, University of Rochester, 601 Elmwood Avenue, Rochester, NY 14642, USA
[4]These authors contributed equally
[5]Lead contact
*Correspondence: martina_poletti@urmc.rochester.edu
https://doi.org/10.1016/j.isci.2026.115168

SUMMARY

Visual crowding—impaired object recognition caused by nearby stimuli—is well documented in peripheral vision and linked to grouping and segmentation. Its spatial extent increases linearly with eccentricity (Bouma's law), consistent with retinal convergence and cortical magnification. Although Bouma's law predicts negligible crowding at the point of fixation, crowding is observed foveally. In the foveola (central 1°), where acuity peaks and photoreceptor-ganglion connectivity is one-to-one, Bouma's law is expected to break, and crowding remain constant. Whether crowding varies across this scale remains unknown. We combined high-resolution eye tracking with gaze-contingent display control to localize gaze and measure crowding thresholds at foveolar eccentricities. Crowding increased linearly within the foveola but with a slope $\approx 3.5\times$ shallower than in the extrafovea. This effect was robust across observers and conservative fixation criteria. Thus, even in the highest-acuity region, integration zones change with eccentricity, arguing against a uniform central fovea and indicating a distinct crowding regime.

INTRODUCTION

Imagine you are driving during rush hour on a crowded urban road. In addition to vehicles, pedestrians and cyclists move in and out of traffic. The constant flow of people and bikes creates a complex visual scene, making it challenging to identify potential hazards or predict their movements. This difficulty arises, in part, from a phenomenon known as visual crowding; recognizing an object becomes harder when it is surrounded by similar stimuli, generally referred to as flankers (see[1–7] for a review on crowding). As the distance between the target and flankers increases, the detrimental effect of crowding is minimized. The smallest distance between the target and flanker at which performance drops by a given amount from the asymptotic performance level is referred to as critical spacing, which defines the spatial extent of the visual crowding effect. However, the extent of crowding is not uniform across the visual field; it depends on the target's eccentricity from the center of gaze, a principle known as Bouma's law.[8,9] According to this law, the extent of visual crowding grows linearly with eccentricity,[8,9]; as the target moves farther away from the center of gaze, the distance between the flankers and the target needs to be increased to maintain similar performance levels across eccentricities.

Visual crowding has been extensively studied in the visual periphery, where its detrimental effects are most pronounced.[1,9] Meanwhile, crowding at the foveal level is thought to have minimal impact on object recognition, as visual acuity is considered the main bottleneck at this scale.[1,2] Although the existence of crowding in the central fovea has been debated over the past 60 years,[2,10,11] there is now mounting evidence showing that crowding influences vision also at the very center of gaze, where acuity is highest.[12–17] Further, the effects of foveal crowding have been reported even when stimuli are presented under diffraction-limited conditions, correcting for optical aberrations, which, under normal viewing conditions, may act as a confounding factor for crowding at this scale.[18,19]

The 1° central fovea, or foveola, is anatomically different from the rest of the retina. It is situated in a pit, free from rods and capillaries, and contains densely packed cone photoreceptors, thus facilitating fine spatial vision.[20] Traditionally, foveolar vision is studied as a unit, and there is limited understanding of how it varies at a sub-degree scale. Visual detection thresholds were found to be relatively uniform within the central foveal region (Domdei et al.,[21] but see Rucci and Poletti[22]). However, recent research has shown that the ability to discriminate fine details is not uniform and drops already 15′ away from the preferred locus of fixation (PLF).[23,24] This raises the question of whether the effects of crowding are the same across the central 1° foveal region or if they are modulated by changes in eccentricity even at this finer scale.

Visual processing in the fovea and periphery is shaped by striking differences in retinal structure and cortical representation. In the fovea, the unique one-to-one mapping between photoreceptors, bipolar cells, and retinal ganglion cells (RGCs)

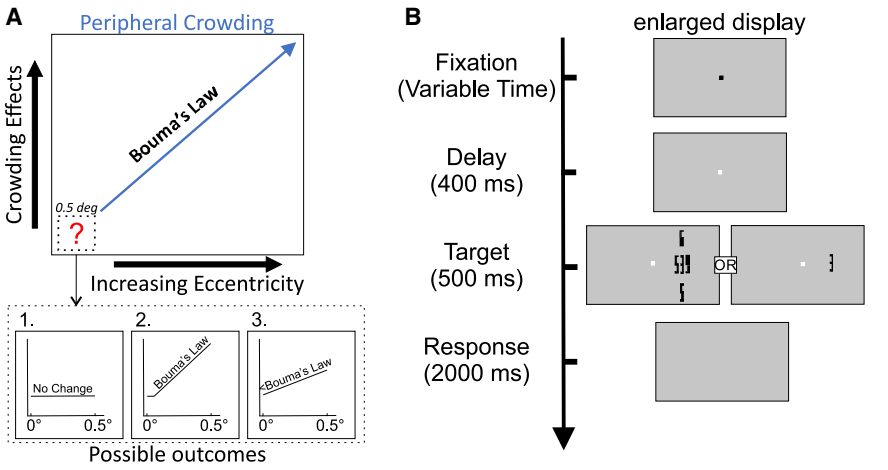

Figure 1. Crowding in the foveola

(A) Illustration of how crowding magnitude increases with eccentricity. Bouma's Law is well known to account for increased crowding effects extrafoveally, yet it is unknown whether and how the magnitude of crowding changes within the central 1° diameter foveola. *Bottom*: three predictions for how the relationship between crowding and eccentricity may unfold within the foveola: (1) Bouma's law breaks in this region, where crowding is still observed and the effects of crowding do not change across the foveola; (2) the region of uniform crowding effects is limited to a small zone around the center of gaze, and beyond this limit, crowding follows the same Bouma's law as extrafoveally; (3) crowding increases with eccentricity within the foveola, but at a slower rate compared to extrafoveally.

(B) Experimental paradigm. Subjects were instructed to identify high-acuity stimuli presented at the center of the display for 500 ms. Stimuli appeared after a brief period of fixation and a 400 ms blank interval in the 0′ eccentricity condition to avoid possible aftereffects of the central fixation dot. Stimuli—digits in Pelli font[12]—varied in size from 0.3′ to 4′ and were presented at eccentricities of 0, 10, 15, or 25 arcminutes. Observers were asked to identify the central digit (the target) among four possible choices.

allows for high-fidelity spatial resolution and color discrimination.[20,25] This high-resolution processing is supported by private-line wiring, where each cone photoreceptor connects to dedicated ON and OFF bipolar cells, which in turn project to distinct midget RGCs (mRGCs), ensuring precise signal transmission and minimal convergence.[26–28] In contrast, the more peripheral retina exhibits significant convergence, where multiple photoreceptors converge onto a single RGC, resulting in spatial pooling that prioritizes sensitivity over fine detail.[25] These retinal differences manifest in the primary visual cortex (V1) as a disproportionate allocation of cortical area to foveal processing, described by the cortical magnification factor (M).[29,30] This measure quantifies how much cortical tissue is devoted to different regions of the visual field, with the fovea receiving vastly more resources compared to the periphery.[31,32] Such cortical organization allows for precise spatial discrimination in foveal vision.[33] In addition to its impact on visual resolution, it has been proposed that RGC convergence and cortical magnification influence visual crowding, with studies suggesting that the spatial extent of crowding may depend on the size of RGC receptive fields[34] and cortical magnification[5,35,36] along the visual pathway. It was unclear until recently whether cortical magnification is uniform within the foveola; however, recent evidence from non-human primates indicates that a cortical magnification gradient is present even within the foveola,[37] and this gradient can potentially affect foveal crowding. Hence, important questions about the specific mechanisms underlying crowding within the fovea remain open.

The discussion on foveal crowding also raises questions about potential differences in the effects and mechanisms of crowding in the 1° central fovea compared to extrafoveal regions. These variations may arise from distinctions in neural architecture at the cortical and/or retinal level and from different functional demands between these retinal regions. The central fovea, optimized for high acuity and fine spatial discrimination, contrasts with the peripheral retina, which exhibits lower spatial resolution but greater sensitivity to motion and temporal change (see Strasburger et al.[2] for a review on this). The structural and functional differences between the foveola and the peripheral visual field suggest that the factors influencing visual crowding may vary between these two regions. Three possible scenarios for how crowding might be characterized within the foveola can be outlined (see Figure 1A): (1) as Bouma's law breaks at the center of gaze, it is conceivable that the impact of crowding does not change with eccentricity within the foveola; (2) alternatively, the region of uniform crowding effects may be limited to the center of gaze and to a small surrounding zone within the foveola. However, beyond this zone, crowding extent may increase with eccentricity within the foveola, following the same Bouma's law as extrafoveally[38]; (3) a third possibility is that the increase in crowding extent with eccentricity is still present in the foveola, but it follows a different regime, possibly reflecting differences in cortical magnification and/or physiological changes between this region and the rest of the retina. In particular, results from Rossi and Roorda[39] suggest that the private-line connection between cones and RGCs is limited to the central 1° diameter region around the preferred retinal locus. A sudden increase in the rate of convergence, which is then reflected in cortical magnification in V1 and beyond, may lead to two distinct crowding regimes in the foveola and extrafoveally.

The foveola is often treated as a functionally uniform region, in part because retinal image quality remains relatively stable across this area,[40–43] and because optical aberrations limit visual resolution to well below the Nyquist sampling limit of the foveal cone mosaic.[39] Further, spotlight sensitivity within the foveola has been reported to be uniform even under diffraction-limited viewing.[21] Yet, cone density changes sharply within the foveola,[21,25,44] fine spatial vision declines with increasing eccentricity within this region,[23,24] and contrast detection has been shown to vary within the foveola under normal viewing conditions in the presence of noise.[24] It therefore remains unclear whether the mechanisms governing higher-order visual

functions, such as grouping and segmentation, operate uniformly across the foveola, or if they are modulated with eccentricity, as happens in the extrafoveal visual field (Figure 1A). To address this question, we examined the phenomenon of visual crowding, a hallmark limitation of object recognition thought to arise from interactions between nearby visual elements. Crowding is likely the result of grouping and segmentation processes,[4] signal pooling, or local integration of visual features.[7,45–47] Previous studies have shown that the central fovea is not immune to crowding[12,14–17,48,49] and that crowding persists even under diffraction-limited conditions achieved with adaptive optics.[18,19] Here, we investigate whether the extent of crowding varies within the foveola under natural viewing conditions—that is, in the presence of physiological higher-order aberrations and fixational eye movements.

Fixational eye movements, though critical for fine vision (see review[22]), pose technical challenges for assessing acuity and crowding near the center of gaze. Eye motion during fixation[17,50–52] and spatial imprecision in video-based eye trackers[53–55] make it difficult to deliver stimuli just a few arcminutes from the foveal center. To overcome this, we used high-precision eye tracking with real-time, gaze-contingent stimulus delivery.[56,57] While retinal stabilization might circumvent these challenges, it imposes highly unnatural viewing conditions, and it leads to a drop in contrast sensitivity.[58] In the current study, we allowed natural fixational eye movements to occur while simultaneously ensuring that stimulation remained confined to the desired eccentricity.

RESULTS

Crowding in the foveola

To measure the effects of crowding across the foveola, visual acuity was first assessed using a 4AFC visual discrimination task. Stimuli consisted of digits in Pelli font, a font specifically designed for testing foveal crowding[12] (Figure 1B). The width of the stimuli ranged from 0.4 to 5 arcminutes, with the height scaled by a factor of 5 (i.e., an aspect ratio of 1:5, width:height, as in Pelli et al.[12]). Stimulus size was adjusted using an adaptive staircase procedure to determine the threshold acuity at each eccentricity.[59] To assess crowding, critical spacing thresholds were measured by surrounding the target with four flanker digits. Flankers were positioned along the horizontal and vertical axes, with center-to-center (c-c) spacing set to 1.4 times the width and height of the target along each axis, respectively. As a result, in the crowded condition, c-c spacing scaled proportionally with stimulus size. Because crowding in this font primarily depends on horizontal spacing, crowding effects are referred to as horizontal c-c spacing. This design allowed us to measure visual acuity in both flanked and unflanked conditions, enabling direct comparison of performance with and without crowding.

Gaze position during stimulus presentation

To ensure precise eye movement measurements and to limit visual stimulation around the desired foveal eccentricity, we employed a high-precision eyetracker[56] coupled with a state-of-the-art, custom-made gaze-contingent display system.[57] The combination of these systems allowed for more accurate gaze localization during the experimental tasks.[22] Figure 2 shows the gaze distribution maps across all tested conditions. To reflect more natural viewing conditions while still ensuring accurate stimulus placement, we allowed for the temporal modulations introduced by fixational eye movements but excluded trials with excessive deviation from the central marker and trials with microsaccades; only trials in which gaze position remained within 30 arcminutes of the center of the display were included in the analysis. As shown in Figure 2, the selected trials, 85.33% ± 7.46% of gaze positions remained within a ± 10 arcminute region around the center of the display. The average Euclidean distance from the display center was 1.03 ± 0.49 arcminutes in the unflanked condition and 1.07 ± 0.50 arcminutes in the crowded condition. A two-way repeated-measures ANOVA with within-subject factors of eccentricity and crowding revealed no significant main effect of crowding on fixation accuracy ($F(3,5) = 0.0008$, $p = 0.98$, $\eta^2 < 0.001$), no significant main effect of eccentricity ($F(3,15) = 0.71$, $p = 0.56$, $\eta^2 = 0.021$), and no interaction between eccentricity and crowding ($F(3,15) = 1.39$, $p = 0.29$, $\eta^2 = 0.0065$). These results indicate that fixation accuracy was comparable in both conditions and across eccentricities. To further assess whether individual differences in fixation stability and crowding extent were related, we computed the bivariate contour ellipse area (BCEA) for each observer and examined its relationship with c-c critical spacing at each eccentricity. BCEA showed no significant relationship with critical spacing at 0′, 15′, or 25′ (all $p > 0.18$), with only a modest effect at 10′ ($R^2 = 0.661$, $p = 0.049$). A linear mixed-effects model likewise revealed no main effect of BCEA ($p = 0.13$) and no significant BCEA × eccentricity interactions (all $p > 0.05$). These results suggest that inter-individual differences in fixation stability did not systematically account for variability in crowding extent.

Effects of crowding on visual acuity

When stimuli were presented in isolation (unflanked) at the PLF, the average stimulus width required to reach threshold performance levels was 1.62′ ± 0.21′, approximately equivalent to 20/16 Snellen acuity. Acuity thresholds in the unflanked condition (isolated stimuli) remained relatively constant across eccentricities (repeated-measures ANOVA: $F(3,15) = 1.05$, $p = 0.399$, $\eta^2 = 0.0007$). The absence of an eccentricity-dependent change in acuity in the unflanked condition may reflect a combination of normal inter-subject variability and limited sample size. In addition, ocular drift may have displaced the stimulus onto retinal locations neighboring the targeted eccentricity, potentially reducing sensitivity to subtle eccentricity-dependent differences in unflanked performance. However, thresholds in the presence of flankers (crowded stimuli) significantly increased with eccentricity (repeated-measures ANOVA: $F(3,15) = 9.56$, $p < 0.001$, $\eta^2 = 0.012$), indicating a systematic degradation in visual acuity under crowded conditions (red circles, Figure 3A) compared to isolated stimulus presentation (blue circles, Figure 3A). As previously shown,[17] at the center of gaze, there was a 29.07% ± 9.42% increase in acuity thresholds (approximately equivalent to 20/20 Snellen acuity) relative to the unflanked condition (two-tailed paired t test, $t(5) = 8.40$, $p = 0.0004$, $BF_{10} = 82.69$, Cohen's $D = 1.93$).

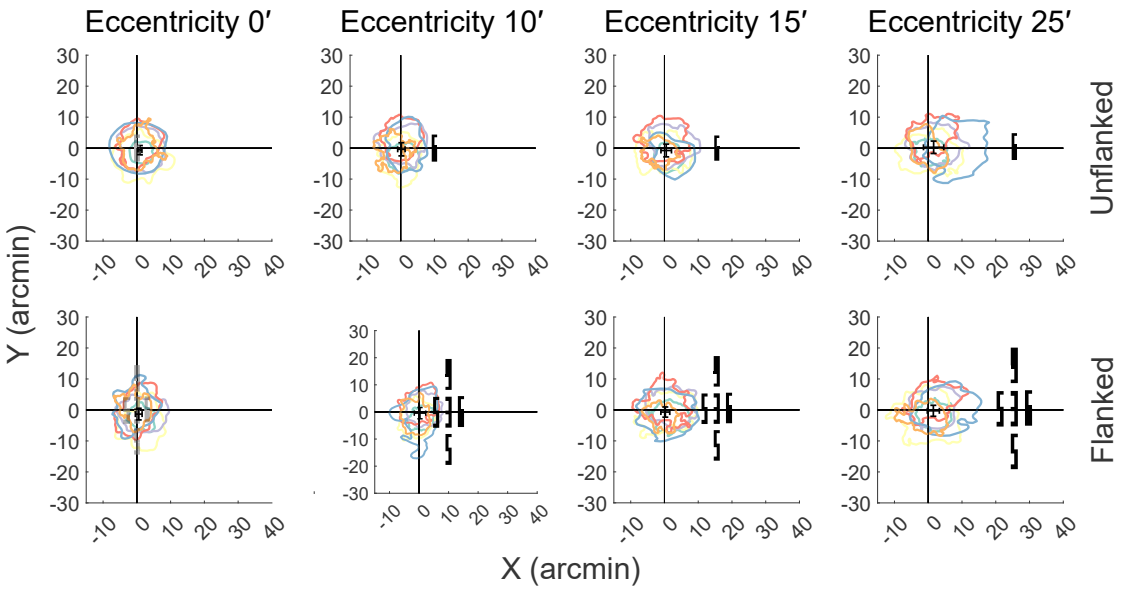

Figure 2. Gaze position during stimulus presentation

Two-dimensional contour plots highlight the area encompassing 68% of gaze positions during stimulus presentation. Gaze distributions for each individual are shown in separate colors for the isolated/unflanked (top row) and flanked (bottom row) conditions during the stimulus presentation interval. Black error bars indicate the mean gaze position with the standard error of the mean (SEM) across subjects in the horizontal and vertical directions. An example stimulus is overlaid in each panel (except at 0′ eccentricity) to illustrate the spatial position of the target relative to the center of the display. The stimulus is scaled based on the average threshold size across subjects in each condition. Individual columns represent the distributions for the different eccentricities tested. When stimuli were presented away from the PLF or >0′ eccentricity, subjects maintained their gaze on the fixation marker, ensuring that retinal stimulation occurred at the desired eccentricity.

A two-way repeated-measures ANOVA with eccentricity and flanker condition as within-subject factors revealed significant main effects of eccentricity ($F(3,15) = 6.43$, $p = 0.0052$, $\eta^2 = 0.068$) and flanker condition ($F(1,5) = 328.42$, $p < 0.001$, $\eta^2 = 0.752$), as well as a significant interaction ($F(3,15) = 9.10$, $p = 0.0011$, $\eta^2 = 0.051$). Post hoc comparisons showed that flanked thresholds were elevated relative to unflanked thresholds at each eccentricity tested (all eccentricities $p < 0.001$). Within the flanked condition, 25′ thresholds were significantly higher than 0' ($p = 0.005$), while other flanked pairwise comparisons and all unflanked comparisons across eccentricities were not significant ($p = 0.057$ and $p = 0.105$, respectively). Flanked visual acuity thresholds increased by 45.4% at 10′, 56.3% at 15′, and 76.1% at 25′ relative to their respective unflanked conditions.[1] Further, we calculated the difference in visual acuity thresholds (in arcminutes) between the flanked and unflanked conditions at each tested eccentricity. When plotting the threshold difference as a function of eccentricity (Figure 3B), all subjects showed consistently positive differences, indicating stronger crowding effects at greater eccentricities. A repeated-measures ANOVA confirmed that crowding strength increased with eccentricity ($F(3,15) = 9.42$, $p < 0.001$, $\eta^2 = 0.085$). Post hoc comparisons revealed that crowding at 15 and 25 arcminutes was significantly greater than at 0 arcminutes ($p = 0.004$ and $p = 0.006$, respectively), while the difference between 0 and 10 arcminutes did not reach significance ($p = 0.171$).

To complement acuity-based measures, we examined critical spacing, the c-c distance between the target and flanker at the acuity threshold, providing a more direct measure of the spatial extent of crowding. We observed a systematic increase in critical spacing measures with increasing stimulus eccentricity (repeated-measures ANOVA: $F(3,15) = 9.56$, $p < 0.001$, $\eta^2 = 0.012$). Post hoc comparisons revealed that critical spacing at 25′ was significantly greater than at 0' ($p = 0.007$), while the differences between 0′ and 10′ and between 0′ and 15′ did not reach significance ($p = 0.067$ and $p = 0.125$, respectively) (Figure 3C). In other words, as eccentricity increased within the foveola, critical spacing (c-c distance) increased from 2.91' ± 0.1′ at the PLF to 4.02' ± 0.16′ at 25′ eccentricity, indicating that flankers needed to be placed farther from the target to maintain similar performance levels.

Beyond measuring the spatial extent of crowding, we compared these values with resolution limits derived from unflanked stimulus thresholds. Specifically, we compared the minimum angle of resolution (MAR), which reflects the limit of visual acuity, to the crowding limit, this time defined as the edge-to-edge (E-E), rather than the c-c, critical spacing threshold (see Figure S1). This allowed us to compare acuity limits with crowding limits across the tested eccentricities within the foveola. The MAR denotes the smallest visual angle (in arcminutes) at which an individual can distinguish two separate points, applicable prior to object recognition. In contrast, E-E critical spacing indicates the spatial range, extending beyond the target area, over which information is pooled for feature integration and object segmentation. Specifically, we compared the acuity thresholds or MAR between the unflanked stimulus condition and the E-E

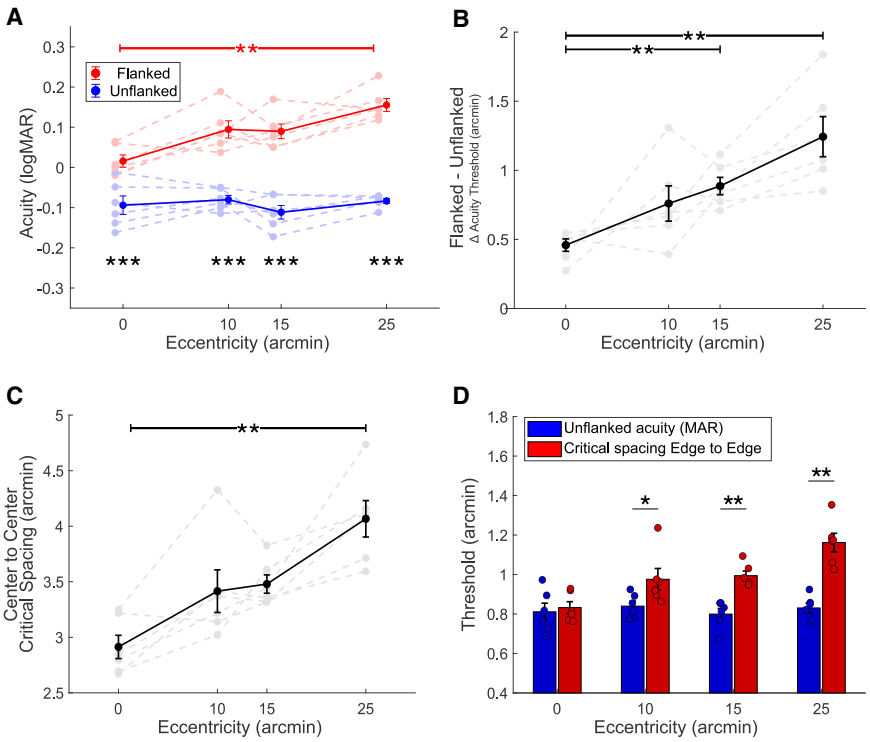

Figure 3. Effects of crowding on visual acuity

(A) Crowded acuity declined with increasing eccentricity (red circles) and remained worse than unflanked acuity (blue circles) at each eccentricity (repeated-measures ANOVA: $p = 0.005$ for eccentricity, $p < 0.001$ for flanker condition, $p = 0.001$ for interaction).

(B) Difference in acuity thresholds between the crowded and unflanked condition for the different eccentricities tested. The difference increased with stimulus eccentricity (repeated-measures ANOVA: $p < 0.001$).

(C) Critical spacing thresholds, represented as the center-to-center separation between the target and the flanker for crowded stimuli, as a function of eccentricity. Similarly, we observed an increase in critical spacing thresholds with eccentricity (repeated-measures ANOVA: $p < 0.001$).

(D) Threshold estimates for unflanked acuity and critical spacing estimates as edge-to-edge spacing for flanked stimuli as a function of eccentricity. Error bars indicate SEM. Asterisks indicate statistically significant post-hoc pairwise comparisons performed using the Tukey-Kramer procedure across eccentricities in (A–C) and significant differences between critical spacing and unflanked MAR at each eccentricity in (D) (*$p < 0.05$, **$p < 0.01$ and ***$p < 0.001$). See also Figures S1 and S3.

critical spacing threshold, which was derived only from flanked trials at the threshold stimulus size, across different eccentricities (Figure 3D). A repeated-measures ANOVA revealed a significant interaction between eccentricity and measure type (E-E spacing vs. MAR), $F(3,15) = 8.82$, $p = 0.0013$, $\eta^2 = 0.0035$), indicating that the relationship between the two measures varied with eccentricity. Post hoc multiple comparisons confirmed that MAR and E-E spacing were comparable at the PLF ($p = 0.41$) but diverged at larger eccentricities ($p = 0.018$, at 10′, $p = 0.002$ at 15′, and $p = 0.002$ at 25′).

Mislocalization errors in the crowded condition

Perceptual mislocalizations, where the target's position is confused with that of a flanker,[60–62] often occur in crowding. In a four-alternative forced-choice task, there are three other possible options for an incorrect response, corresponding to a guess rate for mislocalizations of 33%. If there is an increased probability of responding to one of the flanker locations during incorrect trials, this suggests a bias toward that flanker location (an example for stimuli presented at the center of gaze and at 15′ eccentricity is shown in Figures 4A and 4B). On flanked trials, flankers were selected from a pool of four possible stimulus options with replacement, thus individual stimulus configurations did not necessarily include all four positions options and could contain duplicates. Since the upper and lower flanker locations were equidistant from the center of gaze, we next focused on the directional influence of the inner and outer flanker locations, where the inner flanker was positioned closer to the PLF and the outer flanker was slightly farther from it. Figure 4C shows the probability of reporting either the inner or outer flanker on incorrect trials. We observed a significant effect of eccentricity on mislocalization rates (repeated-measures ANOVA: $F(3,15) = 5.07$, $p = 0.013$, $\eta^2 = 0.005$). Furthermore, there was a significant main effect of mislocalization type, indicating a difference between inner and outer mislocalizations ($F(1,5) = 8.34$, $p = 0.034$, $\eta^2 = 0.028$); the inner flanker was more likely to be mislocalized as the target. However, the interaction between eccentricity and mislocalization type did not reach significance ($F(3,15) = 1.82$, $p = 0.19$, $\eta^2 = 0.01$). Although a contribution of spatial attention in shaping these response biases cannot be ruled out, attention generally reduces, rather than interferes with, target identification and the impact of visual crowding.[63–65] Therefore, it is more likely that these errors originate from an asymmetric averaging of the stimuli surrounding the target, whereby the flanker closer to the PLF dominates the compulsory pooling process underlying crowding.

Foveal and extrafoveal crowding

Overall, these findings indicate that the effects of crowding are not uniform within the foveola. Specifically, the rate of change in critical spacing with eccentricity, quantified as the slope of the fitted function, was ∼ 0.04 within the foveola. This pattern aligns with the third possible outcome proposed in Figure 1A; crowding increases gradually within the foveola rather than remaining constant or showing a sharp discontinuity. Figure 5A shows the change in critical spacing (in arcminutes) as a function of stimulus eccentricity within the foveola. This prompts the question of how this increase compares with the magnitude of crowding effects observed at eccentricities outside the foveola. To address this question, we assessed the rate at which crowding increases from 1° to 6° of eccentricity in 4 subjects (three of whom took part in the main experiment). Outside the boundaries

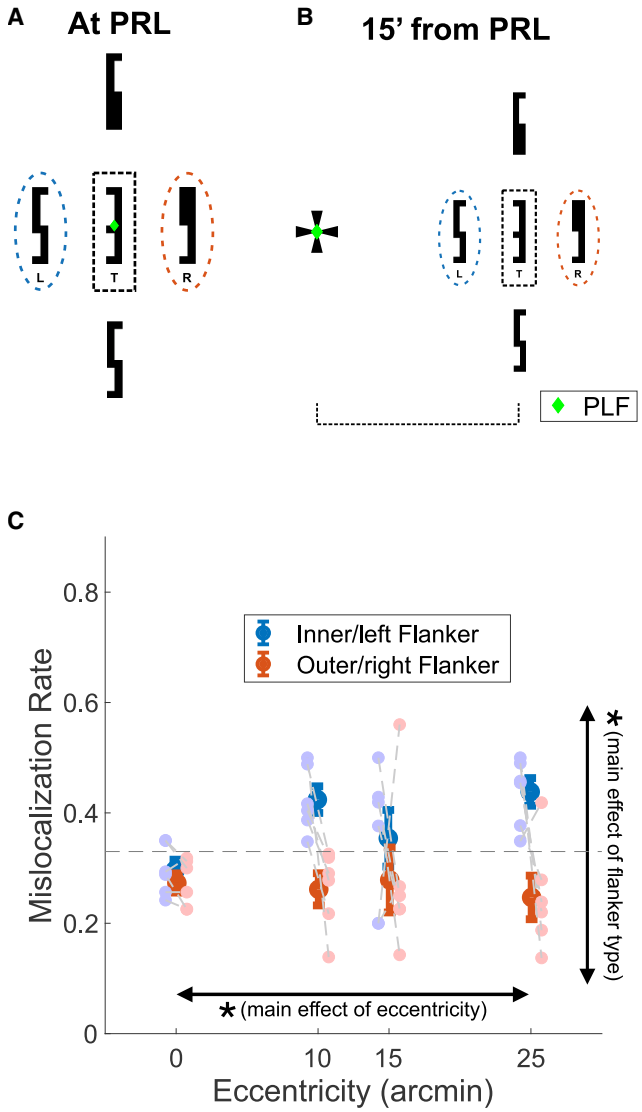

Figure 4. Mislocalization errors in the crowded condition

(A) Illustrates a crowded stimulus presented at the center of gaze (0′ eccentricity), with the target highlighted by a black dashed square. The leftward and rightward flankers are highlighted by blue and orange dashed ovals, respectively. At this eccentricity, the two flankers are equidistant from the preferred locus of fixation.

(B) Depicts a crowded stimulus presented to the right of the center of gaze at 15′ eccentricity. Here, the leftward/inner flanker is slightly closer to the center of gaze compared to the rightward/outer flanker.

(C) The probability of reporting either the inner/left or outer/right flanker as the target in incorrect trials is plotted for each stimulus eccentricity that was tested (repeated-measures ANOVA: $p = 0.013$ for eccentricity, $p = 0.034$). The dashed black line indicates the expected mislocalization rate (33%), corresponding to random guessing among the three incorrect alternatives in a 4AFC task. Error bars indicate SEM. Asterisks denote significant main effects (*$p < 0.05$).

of the foveola, the critical spacing was found to be larger, and the rate of change in critical spacing with eccentricity, quantified as the slope of the fitted function, was also higher (0.149). Figures 5B and 5C shows the relationship between critical spacing (in arcminutes) and eccentricities outside the foveola. Crucially, in the foveola, this rate is approximately 3.5 times smaller than extrafoveally, further highlighting the fact that the foveola is not only a non-uniform region but that crowding processes at this scale follow a different regime compared to extrafoveally.

A piecewise linear fit to eccentricity-level mean data (fovea: 6 subjects; periphery: 4 subjects) revealed a breakpoint at 26.23 arcmin, with a shallow slope in the foveal region (slope = 0.042) and a steeper increase in the peripheral region (slope = 0.149). For the subjects who completed the task both foveally and extrafoveally, we fitted the model individually. At the individual level, breakpoints were more variable and less clearly defined. Nonetheless, all subjects showed an increased rate of crowding growth extrafoveally; however, the eccentricity at which this change occurred varied across participants, with identifiable breakpoints at approximately 22 and 42 arcmin in two subjects, while a clear inflection point could not be reliably determined in the third. To avoid overinterpreting noisy individual fits, we report the group-level model based on the averages of all available subjects at each eccentricity, as it provides a more stable estimate of the foveal-to-peripheral transition. To assess whether a smooth nonlinear transition could also account for the data, we compared piecewise, power-law, and logistic models. All models explained the data well across all eccentricities tested (piecewise $R^2 = 0.998$; power-law $R^2 = 0.997$; logistic $R^2 = 0.996$), but when restricted to the foveal range (<30′), only the piecewise model maintained a strong fit (piecewise $R^2 = 0.94$; power-law $R^2 < 0$; logistic $R^2 < 0$). These results indicate that while smooth nonlinear functions can approximate the overall trend across eccentricities, the piecewise model best captures the distinct scaling behavior within the foveola (see Figure S2).

Extrafoveally the phenomenon of visual crowding is generally characterized by the Bouma fraction, the ratio of critical spacing to eccentricity. Our results show that from 1° to 6° the Bouma fraction remained relatively stable (1°: 0.14 ± 0.02; 2°: 0.16 ± 0.05; 4°: 0.14 ± 0.02; 6°: 0.15 ± 0.02) (see Figure S3), consistent with work showing that the growth of crowding distance with eccentricity is supralinear, but this supralinearity becomes obvious only at much larger eccentricities.[66,67] Interestingly, the Bouma fraction from the current study was generally smaller than those reported in previous studies, where the Bouma fraction was observed to range between 0.4 and 0.5.[8,62] However, a few other studies have reported lower values, around 0.3,[9,10,67,68] and even smaller values for tangential flanker orientation (ranging from 0.1 to 0.2)[1,68] or when using different stimuli.[69] The choice of stimuli (4 out of 9 digits) in our study may have contributed to the lower Bouma factor. Crucially, within the foveola, the Bouma fraction varied with eccentricity (10': 0.35 ± 0.04; 15': 0.23 ± 0.02; 25': 0.16 ± 0.02), showing that foveal crowding cannot be described by a single Bouma fraction value. In the foveola, the Bouma fraction showed a linear decline with eccentricity, with a slope of −0.0118.

To determine whether the pattern of mislocalization observed within the foveola extends into the peripheral visual field, we next analyzed mislocalizations at greater eccentricities (1° to 6°). At more peripheral locations (1°–6°), mislocalization rates did not

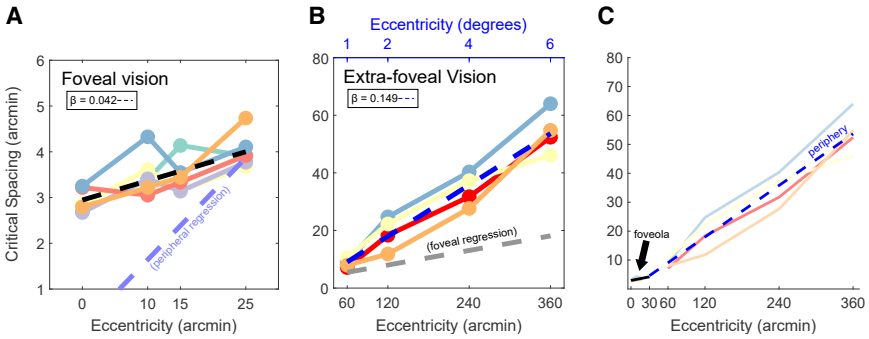

Figure 5. Foveal and extrafoveal crowding

(A) Center-to-center critical spacing as a function of eccentricity in the central fovea. The slope (β) of the fitted line (dashed black line) based on the average data is reported. Individual subjects are represented by different colors. The extrapolated fit based on the extrafoveal data is plotted as a reference.

(B) Four of the same subjects measured in (A) were tested at locations outside the central fovea. Conventions are the same as in (A). The extrapolated fit based on the foveal data is plotted as a reference.

(C) Fits to the crowding growth functions show a markedly shallower foveal slope than extrafoveal. See also Figure S2.

vary significantly with eccentricity ($F(3,9) = 0.95$, $p = 0.46$, $\eta^2 = 0.0023$). In contrast, there was a significant main effect of mislocalization type (inner vs. outer) ($F(1,3) = 15.29$, $p = 0.030$, $\eta^2 = 0.14$), while the interaction between eccentricity and mislocalization type was not significant ($F(3,9) = 0.07$, $p = 0.98$, $\eta^2 = 0.0010$). These results indicate that, unlike the monotonic eccentricity-dependent increase observed in the foveola, peripheral mislocalization errors remain stable across eccentricities, while preserving a consistent directional bias (see Figure S4).

Crowding, acuity, and mRGC spacing

To assess whether the observed acuity and crowding changes reflect retinal sampling limits, we compared our data to a model of mRGC spacing. We used a theoretical model of the spacing between mRGCs in the nasal retina, corresponding to the temporal visual field where stimuli were presented in the foveal and extrafoveal conditions.[70] Using the results shown in Figure 3D, we determined whether the sampling limit of mRGCs could account for the observed results. First, we compared the acuity measures from the unflanked condition across the different eccentricities tested in both the fovea and extrafoveal locations. These comparisons are shown in Figures 6A and 6B, with Figure 6A presenting the foveal data (replicating the results from 3*D*) and Figure 6B showing the results from the extrafoveal condition. Although plotted together for comparison with mRGC spacing, unflanked MAR and E-E critical spacing represent distinct thresholds and are not directly comparable measures. Similarly, we compared the E-E critical spacing measures across eccentricities with the changes in mRGC spacing. Overall, the slope relating mRGC spacing to unflanked visual acuity in the fovea was shallower than the model prediction (0.0001 ± 0.0042 vs. model = 0.0056; $t(5) = -3.22$, $p = 0.023$, $d = 1.32$; $z = -1.99$, $p = 0.046$), which may reflect the influence of habitual optical aberrations that were not corrected in this experiment. In contrast, the slope for E-E critical spacing was steeper (0.0120 ± 0.0055; $t(5) = 2.84$, $p = 0.036$, $d = 1.16$; $z = 2.20$, $p = 0.028$). These findings indicate that mRGC spacing alone is unlikely to account for the observed changes in critical spacing with eccentricity. However, the extrafoveal data showed a closer correspondence between unflanked acuity and mRGC spacing (periphery: mean = 0.0049 ± 0.0013 vs. model = 0.0062; $t(3) = -1.93$, $p = 0.150$, $d = 0.96$; $z = -1.46$, $p = 0.144$), likely because RGC density, rather than optical aberrations, is the limiting factor for acuity at these eccentricities.[39] However, E-E critical spacing increased with eccentricity at a much steeper rate than predicted by mRGC spacing (0.0424 ± 0.0071 vs. model = 0.0062; $t(3) = 10.23$, $p = 0.002$, $d = 5.11$; $z = 1.83$, $p = 0.068$). Thus, while inter-RGC spacing predicts acuity in the extrafovea, it fails to account for crowding, consistent with the idea that crowding and acuity rely on different mechanisms. Notably, prior work has shown that crowding zones subtend a nearly constant number of RGCs across 4° - 18.5°,[34] suggesting that the RGC layout may still provide an appropriate metric for characterizing crowding at larger eccentricities.

DISCUSSION

Here, we investigated the impact of visual crowding across the central 1° foveola while precisely controlling stimulus positioning at subfoveal eccentricities using high-precision eye tracking.[56,57] Although this region is often studied as a single functional unit, our findings provide clear evidence that visual phenomena such as crowding vary systematically with eccentricity, even within this very small part of the visual field. Crowding extent increased linearly with eccentricity in the foveola. Notably, the rate at which crowding magnitude increased with eccentricity was substantially slower than that reported extrafoveally, offering new insights into the distinctions between foveolar and extrafoveolar vision.

Although the existence of crowding in the central fovea has long been debated, there is now compelling evidence that this region is not immune to crowding. Importantly, this implies that Bouma's law breaks at the center of gaze, raising the question of whether crowding effects are uniform within the central fovea, and if not, how the relationship between crowding and eccentricity at the foveal scale differs from the well-characterized increase in crowding with eccentricity in the extrafoveal visual field. Strasburger[38] speculated that there may be a non-linear transition phase near the center of gaze (within 0.2°), where critical spacing increases more gradually before conforming to a linear trend outside this region. Our findings shed light on this by revealing that the intensity of crowding is not uniform across the foveola; the rate of increase with eccentricity is approximately 3.5 times slower foveally than that observed from 1° to 6° outside this

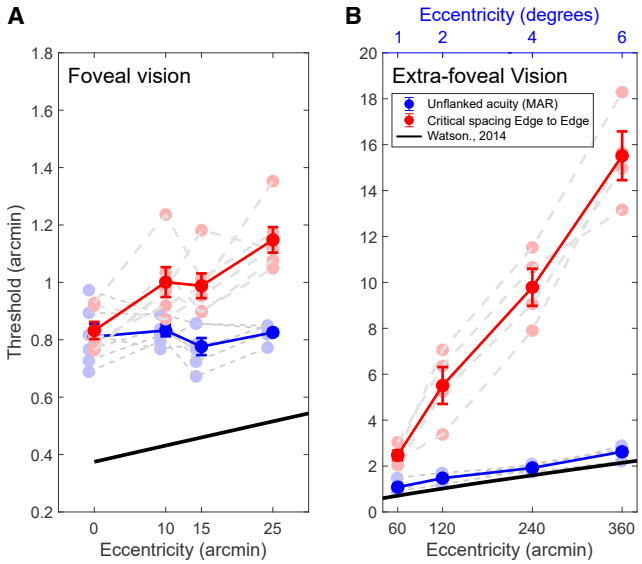

Figure 6. Crowding, acuity, and midget retinal ganglion cell spacing foveally and extrafoveally

Edge-to-edge critical spacing (flanked condition) and visual acuity thresholds (unflanked MAR) for foveal (A) and extrafoveal (B) eccentricities. The solid black line in both panels represents the estimated midget retinal ganglion cell (mRGC) spacing (in arcminutes) based on Watson's model[70]. Error bars indicate SEM. While unflanked visual acuity closely matches mRGC spacing estimates across eccentricities, critical spacing increases more steeply. In the fovea, an offset from the mRGC limit may reflect the effects of habitual optical aberrations.

region (see Figure 5C). Further, our data suggest that there are two phases in the growth of crowding with eccentricity, a slow phase within the boundaries of the foveola and a fast phase outside this region, supporting the idea that crowding follows a distinct scaling regime in the central fovea compared to more eccentric locations. Yet, we acknowledge that the transition between these regimes may be gradual rather than abrupt, and the existence and extent of a potential intermediate "transition zone" between approximately 0.25° and 1° remain open questions for future investigation.

Crowding, often considered a hindrance to visual discrimination, can also be advantageous in natural viewing conditions. While it impairs the ability to distinguish individual elements by integrating information across pooling regions, this integration can facilitate the perception of patterns in visual input.[2,71–73] Gestalt mechanisms, such as grouping, mitigate interference from flanking objects when they are highly similar or aligned, allowing them to be perceived as a unified whole.[74,75] This effect is particularly strong in natural scenes, where multiple objects and textures form coherent structures. At the foveal scale, crowding mechanisms likely aid fine texture discrimination and shape grouping, supporting efficient processing of spatial redundancies. However, foveal crowding can hinder precise recognition tasks, such as reading small text from a distance.

Overall, our findings support a framework in which foveal and peripheral crowding differ primarily in their magnitude and rate of change rather than reflecting distinct mechanisms. Foveally, performance decreases with decreasing flanker spacing, as it does extrafoveally (i.e., we do not observe the facilitation effects reported by other studies at small spacings), and mislocalization errors occur in a similar fashion to those reported extrafoveally. Yet, consistent with previous work,[18] we find that foveal crowding is better characterized by E-E spacing, with E-E spacing thresholds remaining constant independently of stimulus size, whereas extrafoveal crowding is well characterized by c-c thresholds that are independent of stimulus size.[1,3,62,76] Likewise, the Bouma fractions derived from our data (Figure S3) show a steep change within the foveola, followed by a plateau beyond the foveal slope. Further, foveally ocular drifts impact crowding extent,[17,19] whereas this effect is unlikely to occur for extrafoveal crowding. Whether these differences reflect distinct mechanisms for foveal versus extrafoveal crowding remains an open question.

It is important to note that we used the same c-c spacing factor (1.4× target width) for both foveal and peripheral measurements to ensure consistency across eccentricities. This spacing was chosen following Pelli et al.,[12] who showed that a c-c separation of at least 1.4 letter widths prevents overlap masking and allows testing of small spacings without being limited by acuity. Notably, both Pelli et al.[12] and Clark et al.[17] demonstrated that threshold spacing for Pelli-font stimuli remains constant across spacing-to-size ratios, confirming that this configuration yields stable estimates of critical spacing. This design allowed us to directly relate foveal and peripheral thresholds within the same spatial framework. However, it is not yet known whether this spacing-to-size ratio is optimal for assessing extrafoveal crowding with these stimuli. Prior work using stimuli with a 1:1 width-to-height ratio demonstrated that spacing-to-size influences measured crowding strength, producing larger critical spacings and Bouma fractions both foveally and extrafoveally, with an optimal ratio slightly smaller than that used here.[11] Thus, it is possible that extrafoveal crowding is underestimated in the present study, which could account for the overall lower Bouma factors compared to most previous reports. If so, the true difference between the shallow foveolar and steeper peripheral growth of crowding with eccentricity would likely be even greater than what we report here. Importantly, any underestimation of peripheral crowding would only strengthen, rather than weaken, our central conclusion regarding the distinct foveal and extrafoveal regimes of crowding.

Several well-known factors differ between the foveola and the rest of the retina, including visual acuity,[77–79] photoreceptor packing,[25] blood supply,[80] and ganglion cell mapping.[81] Distinct functional channels, such as those associated with the parvocellular and magnocellular pathways, are present throughout the retina, though their relative contributions differ with eccentricity.[81,82] It is possible that the different rate of change of the crowding extent with eccentricity in the central fovea vs. extrafoveally arises from the larger receptive field pooling and the loss of 1-to-1 photoreceptor-to-ganglion cell connections beyond the 1° fovea,[34] leading to broader spatial integration and increased interference from neighboring elements. This difference is likely driven by increased spatial integration outside the foveola due to greater RGC convergence, which leads to increased pooling of visual information.[20,25] In fact, although previous work

suggests that the private line extends beyond the central fovea,[20] work from Rossi and Roorda[39] suggests that it may be limited to a much smaller area, as acuity under diffraction-limited conditions matches cone density only within the central 1° fovea but not outside.

Beyond retinal-level explanations, recent work has emphasized the role of cortical architecture in shaping crowding. The observed increase in critical spacing with eccentricity has been attributed to a reduction in cortical distance between the stimulus representations, reflecting how information is organized in the brain.[5,35,83] It has been proposed that the product of the Bouma function (i.e., radial crowding distance increases linearly with eccentricity) and the cortical magnification function (i.e., radial cortical magnification decreases inversely with eccentricity) is approximately constant,[5] leading to the conservation across eccentricity of the threshold critical spacing on the cortical surface. Consistent with this, Coates et al.[35] demonstrated that in the parafovea, the spatial extent of crowding remains stable when expressed in cortical units. This suggests that cortical distance, shaped by cortical magnification, plays a key role in determining crowding effects, at least extrafoveally. Importantly, recent work has highlighted that the critical cortical crowding distance may not be constant, as initially assumed, but may increase rapidly within the fovea and reach an asymptote only beyond $\approx 5^{\circ}$.[84] Yet, relatively little is known about how visual functions and the cortical magnification gradient are modulated within the central fovea. High-resolution fMRI studies,[37,85] have shown that there is a marked cortical magnification gradient within the foveola. Furthermore, this cortical representation may be amplified beyond what retinal sampling alone predicts.[37,85–89] The degree of this amplification may differ foveally and extrafoveally, contributing to the reported difference in the rate of crowding increase with eccentricity between these regions.

In conclusion, our study demonstrates that visual crowding exhibits a systematic gradient within the central foveola, revealing that even minute increases in eccentricity lead to measurable changes in critical spacing. Interestingly, the rate at which crowding extent increases with eccentricity is 3.5 times slower within the central fovea. These differences likely reflect complementary retinal and cortical contributions, whose impact may differ across spatial scales. Ultimately, these results show that central foveal vision is less uniform than previously assumed and that the eccentricity-dependent increase in crowding at this scale is governed by a distinct regime.

Limitations of the study

This study focused on fine-scale measurements of visual crowding within the central foveola and adjacent peripheral locations using a specific stimulus type. While this approach enabled precise characterization of eccentricity-dependent changes in crowding, we did not densely sample intermediate eccentricities between 0.5° and 1°, limiting the direct empirical determination of the inflection point at which crowding transitions to a steeper peripheral growth regime. In addition, although results were consistent across observers, the sample size limits the assessment of potential individual differences, including effects related to sex or other demographic factors. Finally, crowding was measured using high-acuity digit stimuli under controlled fixation conditions; whether similar scaling properties generalize to other stimulus types, tasks, or more natural viewing conditions remains to be determined.

RESOURCE AVAILABILITY

Lead contact

Further information and requests for resources should be directed to and will be fulfilled by the lead contact, Martina Poletti (martina_poletti@urmc.rochester.edu).

Materials availability

This study did not generate new unique reagents.

Data and code availability

- Human behavioral data have been deposited at https://doi.org/10.17605/OSF.IO/E9K6Q and are publicly available as of the date of publication.
- All original code has been deposited at https://doi.org/10.17605/OSF.IO/E9K6Q and is publicly available as of the date of publication.
- Any additional information required to reanalyze the data reported in this paper is available from the lead contact upon request.

ACKNOWLEDGMENTS

This work was supported by the National Institutes of Health grants R01 EY029788 (to M.P.) and by NIH EY001319 to the Center for Visual Science at the University of Rochester.

AUTHOR CONTRIBUTIONS

A.M.C. and M.P. designed the study. A.M.C. collected the data. A.M.C., K.S.P., and M.P. analyzed the data and wrote the manuscript.

DECLARATION OF INTERESTS

The authors declare no competing interests.

DECLARATION OF GENERATIVE AI AND AI-ASSISTED TECHNOLOGIES IN THE WRITING PROCESS

During the preparation of this work, the authors used ChatGPT for language editing and clarity checks only. The authors reviewed and edited the content and take full responsibility for the final manuscript.

STAR★METHODS

Detailed methods are provided in the online version of this paper and include the following:

- KEY RESOURCES TABLE
- EXPERIMENTAL MODEL AND STUDY PARTICIPANT
- METHOD DETAILS
  - Stimuli and apparatus
  - Experimental paradigm
  - Refractive correction
- QUANTIFICATION AND STATISTICAL ANALYSIS
  - Data analysis
  - Estimation of acuity thresholds
  - Statistical analysis
  - Pairwise comparisons
  - Reporting summary

SUPPLEMENTAL INFORMATION

Supplemental information can be found online at https://doi.org/10.1016/j.isci.2026.115168.

Received: September 25, 2025
Revised: December 18, 2025
Accepted: February 24, 2026
Published: March 2, 2026

REFERENCES

1. Levi, D.M. (2008). Crowding—An essential bottleneck for object recognition: A mini-review. Vision Res. *48*, 635–654.
2. Strasburger, H., Rentschler, I., and Jüttner, M. (2011). Peripheral vision and pattern recognition: A review. J. Vis. *11*, 13.
3. Whitney, D., and Levi, D.M. (2011). Visual crowding: a fundamental limit on conscious perception and object recognition. Trends Cogn. Sci. *15*, 160–168.
4. Herzog, M.H., Sayim, B., Chicherov, V., and Manassi, M. (2015). Crowding, grouping, and object recognition: A matter of appearance. J. Vis. *15*, 5.
5. Pelli, D.G. (2008). Crowding: A cortical constraint on object recognition. Curr. Opin. Neurobiol. *18*, 445–451.
6. Lonnqvist, B., Clarke, A.D.F., and Chakravarthi, R. (2020). Crowding in humans is unlike that in convolutional neural networks. Neural Netw. *126*, 262–274.
7. Rosenholtz, R. (2016). Capabilities and Limitations of Peripheral Vision. Annu. Rev. Vis. Sci. *2*, 437–457.
8. Bouma, H. (1970). Interaction effects in parafoveal letter recognition. Nature *226*, 177–178.
9. Toet, A., and Levi, D.M. (1992). The two-dimensional shape of spatial interaction zones in the parafovea. Vision Res. *32*, 1349–1357.
10. Strasburger, H., Harvey, L.O., and Rentschler, I. (1991). Contrast thresholds for identification of numeric characters in direct and eccentric view. Percept. Psychophys. *49*, 495–508.
11. Song, S., Levi, D.M., and Pelli, D.G. (2014). A double dissociation of the acuity and crowding limits to letter identification, and the promise of improved visual screening. J. Vis. *14*, 3.
12. Pelli, D.G., Waugh, S.J., Martelli, M., Crutch, S.J., Primativo, S., Yong, K.X., Rhodes, M., Yee, K., Wu, X., Famira, H.F., et al. (2016). A clinical test for visual crowding. F1000Res. *5*, 81.
13. Flom, M.C., Weymouth, F.W., and Kahneman, D. (1963). Visual Resolution and Contour Interaction. JOSA *53*, 1026–1032.
14. Coates, D.R., and Levi, D.M. (2014). Contour interaction in foveal vision: a response to siderov, waugh, and bedell (2013). Vision Res. *96*, 140–144.
15. Siderov, J., Waugh, S.J., and Bedell, H.E. (2013). Foveal contour interaction for low contrast acuity targets. Vision Res. *77*, 10–13.
16. Bondarko, V.M., Chikhman, V.N., Danilova, M.V., and Solnushkin, S.D. (2024). Foveal crowding for large and small Landolt Cs: Similarity and Attention. Vision Res. *215*, 108346.
17. Clark, A.M., Huynh, A., and Poletti, M. (2024). Oculomotor Contributions to Foveal Crowding. J. Neurosci. *44*, e0594242024.
18. Coates, D.R., Levi, D.M., Touch, P., and Sabesan, R. (2018). Foveal Crowding Resolved. Sci. Rep. *8*, 9177.
19. Prahalad, K.S., Clark, A.M., Moon, B., Roorda, A., Tiruveedhula, P., Harmening, W., Gutnikov, A., Jenks, S.K., Kapisthalam, S., Rucci, M., et al. (2025). Non-uniform signal pooling across the foveola. Curr. Biol. *35*, 6086–6099.e4.
20. Kolb, H., Nelson, R.F., Ahnelt, P.K., Ortuño-Lizarán, I., and Cuenca, N. (1995). The Architecture of the Human Fovea. In Webvision: Org. Retina Vis. Syst., H. Kolb, E. Fernandez, and R. Nelson, eds University of Utah Health Sciences Center.
21. Domdei, N., Reiniger, J.L., Holz, F.G., and Harmening, W.M. (2021). The Relationship Between Visual Sensitivity and Eccentricity, Cone Density and Outer Segment Length in the Human Foveola. Investig. Ophthalmol. Vis. Sci. *62*, 31.
22. Rucci, M., and Poletti, M. (2015). Control and functions of fixational eye movements. Annu. Rev. Vis. Sci. *1*, 499–518.
23. Poletti, M., Listorti, C., and Rucci, M. (2013). Microscopic Eye Movements Compensate for Nonhomogeneous Vision within the Fovea. Curr. Biol. *23*, 1691–1695.
24. Intoy, J., Mostofi, N., and Rucci, M. (2021). Fast and nonuniform dynamics of perisaccadic vision in the central fovea. Proc. Natl. Acad. Sci. USA *118*, e2101259118.
25. Curcio, C.A., Sloan, K.R., Kalina, R.E., and Hendrickson, A.E. (1990). Human photoreceptor topography. J. Comp. Neurol. *292*, 497–523.
26. Boycott, B.B., Dowling, J.E., and Kolb, H. (1969). Organization of the Primate Retina: Light Microscopy. Phil. Trans. R. Soc. London. Series B, Biological Sciences *255*, 109–184.
27. Calkins, D.J., Schein, S.J., Tsukamoto, Y., and Sterling, P. (1994). M and L cones in macaque fovea connect to midget ganglion cells by different numbers of excitatory synapses. Nature *371*, 70–72.
28. Polyak, S.L. (1941). The Retina (Univ. Chicago Press).
29. Daniel, P.M., and Whitteridge, D. (1961). The representation of the visual field on the cerebral cortex in monkeys. J. Physiol. *159*, 203–221.
30. Van Essen, D.C., Newsome, W.T., and Maunsell, J.H. (1984). The visual field representation in striate cortex of the macaque monkey: Asymmetries, anisotropies, and individual variability. Vision Res. *24*, 429–448.
31. Tootell, R.B., Silverman, M.S., Switkes, E., and De Valois, R.L. (1982). Deoxyglucose Analysis of Retinotopic Organization in Primate Striate Cortex. Science *218*, 902–904.
32. Cowey, A., and Rolls, E.T. (1974). Human cortical magnification factor and its relation to visual acuity. Exp. Brain Res. *21*, 447–454.
33. Drasdo, N. (1991). Neural substrates and threshold gradients of peripheral vision. Limits of vision *5*, 251–276.
34. Kwon, M., and Liu, R. (2019). Linkage between retinal ganglion cell density and the nonuniform spatial integration across the visual field. Proc. Natl. Acad. Sci. USA *116*, 3827–3836.
35. Coates, D.R., Jiang, X., Levi, D.M., and Sabesan, R. (2022). Cortical distance unifies the extent of parafoveal contour interactions. J. Vis. *22*, 15.
36. Pelli, D.G., and Tillman, K.A. (2008). The uncrowded window of object recognition. Nat. Neurosci. *11*, 1129–1135.
37. Qian, M., Wang, J., Gao, Y., Chen, M., Liu, Y., Zhou, D., Lu, H.D., Zhang, X., Hu, J.M., and Roe, A.W. (2024). Multiple loci for foveolar vision in macaque monkey visual cortex. Nat. Neurosci. *28*, 137–149.
38. Strasburger, H. (2020). Seven myths on crowding and peripheral vision. Iperception. *11*, 2041669520913052.
39. Rossi, E.A., and Roorda, A. (2010). The relationship between visual resolution and cone spacing in the human fovea. Nat. Neurosci. *13*, 156–157.
40. Liang, J., Williams, D.R., and Miller, D.T. (1997). Supernormal vision and high-resolution retinal imaging through adaptive optics. JOSA A *14*, 2884–2892.
41. Tarrant, J., and Roorda, A. (2006). The Extent of the Isoplanatic Patch of the Human Eye. Investig. Ophthalmol. Vis. Sci. *47*, 1195.
42. Bedggood, P., Daaboul, M., Ashman, R., Smith, G., and Metha, A. (2008). Characteristics of the human isoplanatic patch and implications for adaptive optics retinal imaging. J. Biomed. Opt. *13*, 024008.
43. Huang, X., Hargrave, A., Bentley, J., and Dubra, A. (2024). Biometry study of foveal isoplanatic patch variation for adaptive optics retinal imaging. Biomed. Opt. Express *15*, 5674–5690.
44. Reiniger, J.L., Domdei, N., Holz, F.G., and Harmening, W.M. (2021). Human gaze is systematically offset from the center of cone topography. Curr. Biol. *31*, 4188–4193.e3.

45. Greenwood, J.A., Bex, P.J., and Dakin, S.C. (2010). Crowding changes appearance. Curr. Biol. *20*, 496–501.
46. Harrison, W.J., and Bex, P.J. (2015). A Unifying Model of Orientation Crowding in Peripheral Vision. Curr. Biol. *25*, 3213–3219.
47. Rosenholtz, R., Yu, D., and Keshvari, S. (2019). Challenges to pooling models of crowding: implications for visual mechanisms. J. Vis. *19*, 15–25.
48. Flom, M.C., Heath, G.G., and Takahashi, E. (1963). Contour Interaction and Visual Resolution: Contralateral Effects. Science *142*, 979–980.
49. Shamsi, F., Liu, R., and Kwon, M. (2022). Foveal crowding appears to be robust to normal aging and glaucoma unlike parafoveal and peripheral crowding. J. Vis. *22*, 10.
50. Steinman, R.M., and Collewijn, H. (1980). Binocular retinal image motion during active head rotation. Vision Res. *20*, 415–429.
51. Rucci, M., and Victor, J.D. (2015). The unsteady eye: An information-processing stage, not a bug. Trends Neurosci. *38*, 195–206.
52. Cherici, C., Kuang, X., Poletti, M., and Rucci, M. (2012). Precision of sustained fixation in trained and untrained observers. J. Vis. *12*, 31.
53. Ehinger, B.V., Groß, K., Ibs, I., and König, P. (2019). A new comprehensive eye-tracking test battery concurrently evaluating the Pupil Labs glasses and the EyeLink 1000. PeerJ *7*, e7086.
54. Holmqvist, K., Nyström, M., Andersson, R., Dewhurst, R., Jarodzka, H., and Weijer, J.V.D. (2011). Eye Tracking: A Comprehensive Guide to Methods and Measures (Lund Eye-Tracking Research Institute).
55. Blignaut, P., and Wium, D. (2014). Eye-tracking data quality as affected by ethnicity and experimental design. Behav. Res. Methods *46*, 67–80.
56. Wu, R.-J., Clark, A.M., Cox, M.A., Intoy, J., Jolly, P.C., Zhao, Z., and Rucci, M. (2023). High-resolution eye-tracking via digital imaging of Purkinje reflections. J. Vis. *23*, 4.
57. Santini, F., Redner, G., Iovin, R., and Rucci, M. (2007). EyeRIS: A general-purpose system for eye-movement-contingent display control. Behav. Res. Methods *39*, 350–364.
58. Intoy, J., Li, Y.H., Bowers, N.R., Victor, J.D., Poletti, M., and Rucci, M. (2024). Consequences of eye movements for spatial selectivity. Curr. Biol. *34*, 3265–3272.e4.
59. Taylor, M.M., and Creelman, C.D. (1967). PEST: Efficient Estimates on Probability Functions. J. Acoust. Soc. Am. *41*, 782–787.
60. Greenwood, J.A., Bex, P.J., and Dakin, S.C. (2009). Positional averaging explains crowding with letter-like stimuli. Proc. Natl. Acad. Sci. USA *106*, 13130–13135.
61. Parkes, L., Lund, J., Angelucci, A., Solomon, J.A., and Morgan, M. (2001). Compulsory averaging of crowded orientation signals in human vision. Nat. Neurosci. *4*, 739–744.
62. Pelli, D.G., Palomares, M., and Majaj, N.J. (2004). Crowding is unlike ordinary masking: Distinguishing feature integration from detection. J. Vis. *4*, 1136–1169.
63. Yeshurun, Y., and Rashal, E. (2010). Precueing attention to the target location diminishes crowding and reduces the critical distance. J. Vis. *10*, 16.
64. Kewan-Khalayly, B., Migó, M., and Yashar, A. (2022). Transient attention equally reduces visual crowding in radial and tangential axes. J. Vis. *22*, 3.
65. Gong, M., Liu, T., Liu, X., Huangfu, B., and Geng, F. (2023). Attention relieves visual crowding: Dissociable effects of peripheral and central cues. J. Vis. *23*, 9.
66. Coates, D.R., Ludowici, C.J.H., and Chung, S.T.L. (2021). The generality of the critical spacing for crowded optotypes: From Bouma to the 21st century. J. Vis. *21*, 18.
67. Kurzawski, J.W., Burchell, A., Thapa, D., Winawer, J., Majaj, N.J., and Pelli, D.G. (2023). The Bouma law accounts for crowding in 50 observers. J. Vis. *23*, 6.
68. Chung, S.T., Levi, D.M., and Legge, G.E. (2001). Spatial-frequency and contrast properties of crowding. Vision Res. *41*, 1833–1850.
69. Harrison, W.J., and Bex, P.J. (2014). Integrating Retinotopic Features in Spatiotopic Coordinates. J. Neurosci. *34*, 7351–7360.
70. Watson, A.B. (2014). A formula for human retinal ganglion cell receptive field density as a function of visual field location. J. Vis. *14*, 15.
71. Korte, W. (1923). Über die Gestaltauffassung im indirekten Sehen. Z. Psychol. *93*, 17–82.
72. Banks, W.P., Larson, D.W., and Prinzmetal, W. (1979). Asymmetry of visual interference. Percept. Psychophys. *25*, 447–456.
73. Herzog, M.H., and Manassi, M. (2015). Uncorking the bottleneck of crowding: A fresh look at object recognition. Curr. Opin. Behav. Sci. *1*, 86–93.
74. Manassi, M., Sayim, B., and Herzog, M.H. (2012). Grouping, pooling, and when bigger is better in visual crowding. J. Vis. *12*, 13.
75. Manassi, M., Sayim, B., and Herzog, M.H. (2013). When crowding of crowding leads to uncrowding. J. Vis. *13*, 10.
76. Tripathy, S.P., and Cavanagh, P. (2002). The extent of crowding in peripheral vision does not scale with target size. Vision Res. *42*, 2357–2369.
77. Weymouth, F.W. (1958). Visual sensory units and the minimal angle of resolution. Am. J. Ophthalmol. *46*, 102–113.
78. Rovamo, J., and Virsu, V. (1979). An estimation and application of the human cortical magnification factor. Exp. Brain Res. *37*, 495–510.
79. Anderson, S.J., Mullen, K.T., and Hess, R.F. (1991). Human peripheral spatial resolution for achromatic and chromatic stimuli: limits imposed by optical and retinal factors. J. Physiol. *442*, 47–64.
80. Provis, J.M. (2001). Development of the Primate Retinal Vasculature. Prog. Retin. Eye Res. *20*, 799–821.
81. Dacey, D.M. (1993). The mosaic of midget ganglion cells in the human retina. J. Neurosci. *13*, 5334–5355.
82. Wässle, H. (2004). Parallel processing in the mammalian retina. Nat. Rev. Neurosci. *5*, 747–757.
83. Levi, D.M., Klein, S.A., and Aitsebaomo, A.P. (1985). Vernier acuity, crowding and cortical magnification. Vision Res. *25*, 963–977.
84. Strasburger, H. (2022). On the cortical mapping function – Visual space, cortical space, and crowding. Vision Res. *194*, 107972.
85. Schira, M.M., Tyler, C.W., Breakspear, M., and Spehar, B. (2009). The Foveal Confluence in Human Visual Cortex. J. Neurosci. *29*, 9050–9058.
86. Azzopardi, P., and Cowey, A. (1993). Preferential representation of the fovea in the primary visual cortex. Nature *361*, 719–721.
87. Azzopardi, P., and Cowey, A. (1996). Models of ganglion cell topography in the retina of macaque monkeys and their application to sensory cortical scaling. Neuroscience *72*, 617–625.
88. Azzopardi, P., and Cowey, A. (1996). The overrepresentation of the fovea and adjacent retina in the striate cortex and dorsal lateral geniculate nucleus of the macaque monkey. Neuroscience *72*, 627–639.
89. Adams, D.L., and Horton, J.C. (2003). A Precise Retinotopic Map of Primate Striate Cortex Generated from the Representation of Angioscotomas. J. Neurosci. *23*, 3771–3789.
90. Crane, H.D., and Steele, C.M. (1985). Generation-V dual-Purkinje-image eyetracker. Appl. Opt. *24*, 527.
91. Ko, H.-k., Snodderly, D.M., and Poletti, M. (2016). Eye movements between saccades: Measuring ocular drift and tremor. Vision Res. *122*, 93–104.
92. Baron, W.S., and Westheimer, G. (1973). Visual acuity as a function of exposure duration. J. Opt. Soc. Am. *63*, 212–219.
93. McAnany, J.J. (2014). The effect of exposure duration on visual acuity for letter optotypes and gratings. Vision Res. *105*, 86–91.
94. Intoy, J., and Rucci, M. (2020). Finely tuned eye movements enhance visual acuity. Nat. Commun. *11*, 795.
95. Atchison, D.A., Bradley, A., Thibos, L.N., and Smith, G. (1995). Useful variations of the Badal optometer. Optom. Vis. Sci. *72*, 279–284.
96. Wichmann, F.A., and Hill, N.J. (2001). The psychometric function: I. Fitting, sampling, and goodness of fit. Percept. Psychophys. *63*, 1293–1313.

STAR★METHODS

KEY RESOURCES TABLE

REAGENT or RESOURCE	SOURCE	IDENTIFIER
Deposited data		
Original psychophysics data	This paper	https://osf.io/e9k6q/overview?view_only=aa932ee788b0434ebb17d16e44b25de6
Software and algorithms		
Custom MATLAB code for data analysis and figure generation	This paper	https://osf.io/e9k6q/overview?view_only=aa932ee788b0434ebb17d16e44b25de6
MATLAB (R2022b)	Mathworks	https://www.mathworks.com/RRID: SCR_001622
BayesFactor MATLAB toolbox	Lab of Cognitive Neuroscience, K-Lab	https://github.com/klabhub/bayesFactor
psignifit 4	Wichmann Lab	https://github.com/wichmann-lab/psignifit

EXPERIMENTAL MODEL AND STUDY PARTICIPANT

Six participants with normal vision took part in the study, including five naive observers and one experienced observer who was also an author. The group comprised 2 males and 4 females, aged between 18 and 29 years. Participants were human adults (Homo sapiens) with normal or corrected-to-normal vision and were excluded if they reported a history of ocular disease, neurological disorders, or language-related disorders (e.g., dyslexia, hyperlexia, aphasia), consistent with the approved study protocol. Exclusion criteria were based on self-report during screening. During the initial screening, all participants demonstrated at least 20/20 Snellen acuity with or without the need for corrective lenses. All six participants completed the foveal crowding measurements. Four participants completed the extrafoveal condition; of these, three completed the foveal task, whereas one participant contributed only extrafoveal data due to the impossibility of estimating reliable thresholds in the foveal condition. Thus, allocation to experimental conditions was determined by successful threshold convergence and data quality. Ethical approval for this research study was obtained from the University of Rochester's Research Subjects Review Board (Study ID: *STUDY*00001477). Subjects attended an initial screening session, which involved a comprehensive explanation of the experimen t and a thorough review of the consent form materials. After understanding the information and voluntarily agreeing to participate, informed consent was obtained and documented. Every effort was made to recruit participants representative of the racial and ethnic composition of the local population, consistent with the study protocol. Due to the small sample size, the study was not powered to examine potential effects of sex or gender on the results, and no sex-based analyses were performed.

METHOD DETAILS

Stimuli and apparatus

Stimuli were presented monocularly to the right eye while the left eye was covered. Eye movements were recorded with high precision using a custom-made digital Dual Purkinje Image (dDPI) eye tracker,[56] operating at a sampling rate of 340Hz. This system had minimal internal noise (below 1 arcminute) and a spatial resolution of at least 1 arcminute.[56,90,91] To minimize noise and enhance eye-tracking precision, the observer's head was immobilized with a dental-imprint bite bar and head-holder. The stimuli were displayed on an ASUS PG258Q LCD monitor with a vertical refresh rate of 200Hz and a spatial resolution of 1920 x 1080 pixels. The monitor was positioned at either 3 or 5 m from the observer, corresponding to pixel sizes of 0.25 arcminutes and 0.19 arcminutes, respectively.

Stimuli consisted of digits (3, 5, 6, and 9) from the Pelli number-font[12] and were presented individually at the center of the display for 500 ms. This duration is sufficient to reach plateau performance with high-contrast stimuli,[92,93] and it is comparable to the average fixation duration in a self-paced acuity task.[94] Therefore, this presentation duration ensures that crowding thresholds reflect the observer's maximal performance while retaining the physiological temporal modulations introduced by ocular drift during a normal viewing condition in the presence of high-acuity stimuli. The Pelli number font is specifically designed to test crowding within the fovea. Its vertically elongated design (aspect ratio 5:1) allows for a smaller center-to-center separation between the target and flanker compared to fonts with equal aspect ratios, thus providing a robust estimate of crowding thresholds. It has further been shown that the critical spacing estimates using the font are independent from the spacing-to-size ratio within the fovea,[12] also reconfirmed by our previous work.[17] On flanked trials, flankers were randomly selected from a pool of four possible digit options with replacement, such that individual configurations could include duplicate digits, including cases where one or both flankers matched the target. This

ensured full randomization and prevented any systematic pairing of target-flanker identities. Flankers were positioned along both the horizontal and vertical axes to maintain consistency with standard crowding paradigms and to match configurations commonly used in peripheral crowding studies. However, crowding was likely primarily driven by horizontally aligned (radial) flankers, with vertically aligned (tangential) flankers contributing minimally.[12] The stimuli were presented at maximum contrast in black text on an uniform gray background and were controlled using EyeRIS,[57] a custom-developed system enabling gaze-contingent display control. Stimuli were presented either at the center of the display (0′ eccentricity) or at one of three other eccentricities to the right or left of the center of gaze (10′, 15′, 25′). On trials where stimuli appeared at the center of the display (0′ eccentricity), in addition to the stimulus we presented four peripheral arches centered on the target to help subjects maintain their gaze near the center. On the other hand, when stimuli were presented away from the center of gaze, a 10x10 arcminute fixation marker appeared at the center of the display to facilitate precise fixation behavior. When flankers were present, the separation between the edge of the target and the flanker (flanker spacing) was set to be 1.4 times the width of the stimulus (spacing-to-size ratio or nominal spacing). To compute the corresponding edge-to-edge (E–E) spacing, we first determined the center-to-center spacing between the target and flanker at threshold, and then subtracted half the target width and half the flanker width (i.e., the stimulus width), yielding the true E–E spacing.

Experimental paradigm

Data collection involved multiple experimental sessions, each lasting about 1 hour, with each subject completing an average of 5 sessions. Each session commenced with setup operations to ensure optimal observer positioning and eye tracker calibration. A two-step gaze-contingent calibration procedure was performed to map the eye tracker's output to visual angles, enhancing the localization of the preferred retinal locus of fixation. During the first phase (automatic calibration), observers sequentially fixated on a 3x3 grid, while the second phase (manual calibration) allowed observers to confirm or refine the calibration by fixating on the same grid points while manually adjusting a gaze contingent marker to overlap with their gaze direction at each location. Before each trial, manual calibration was repeated for the central position to compensate for possible head movements.

Each trial began with a 10x10 arcminute fixation point at the screen center, followed by a 400 ms delay to prevent aftereffects from the fixation point. The target stimulus was then presented, and participants identified it by selecting one of four possible digits using a remote controller. Fixation trials, in which participants maintained fixation on a 10x10 arcminute marker at the display center, were interspersed approximately every 30–50 task trials, with subjects instructed to maintain fixation for 2–5 s. Target acuity and crowding threshold (critical spacing) was determined using the Parametric Estimation by Sequential Testing (PEST) procedure,[59] where both the target size and flanker spacing changed based on subject's performance which was set to converge at 62.5% for a 4AFC task.

All subjects started the initial experimental session with the stimuli presented at the center of gaze in the uncrowded condition. After the first 100 trial block, condition blocks where then randomized by eccentricity (either presented at 0, 10, 15, or 25 eccentricity temporally) and crowding condition (unflanked or crowded). All subjects were run on each unique block type at least twice to ensure repeatable thresholds estimates. A subset of subjects was also tested in the nasal visual field; however, because no systematic differences were observed between nasal and temporal thresholds, we restricted our analysis to the temporal dataset.

Refractive correction

In the current study, we employed a badal lens setup to compensate for spherical refractive error. This device allows participants to make precise adjustments, correcting for different amounts of spherical defocus and achieving high acuity vision. The Badal lens modifies the effective focal length of the lens system, ensuring that all stimuli are presented at the same size in visual angle by accounting for the introduced magnification factor.

To guide the correction process, we used the Atchison's model[95] for our Badal lens. This model describes a relay system that helps achieve accurate corrections with limited distortions. Participants utilized this guidance to correct for varying amounts of spherical defocus and achieve corrections to 20/20 vision or better. Additionally, to assist participants in their subjective correction, we integrated a duo-chrome test with a red and green screen. Subjects ensured that the target was equally clear on both the red and green backgrounds before proceeding. This measure facilitated the fine-tuning of visual adjustments, contributing to the accuracy of participants' corrective experiences throughout the study.

QUANTIFICATION AND STATISTICAL ANALYSIS

Data analysis

Eye Movements: Eye movements were categorized as saccades (including microsaccades) and ocular drift. Automatic classification was followed by a manual review by an expert experimenter. Trials with saccades, blinks, or poor tracking during stimulus presentation were excluded. On the other hand, when stimuli were presented away from the center of gaze (eccentricities 10, 15 and 25 arcminutes), trials where the gaze position deviated more than 30 arcminutes from the central fixation point were discarded. Ocular drift was examined during fixation periods far from saccades or blinks, revealing stationary behavior with consistent speed. On average, 32.8% ± 23.7% of trials were discarded across subjects based on these criteria. The same exclusion was used for the larger eccentricities tested (1–6°).

Estimation of acuity thresholds

Visual acuity was calculated both as units of stimulus width (arcminutes) and as minimum angle of resolution (MAR). Visual acuity thresholds, representing the minimum stimulus width for reliable performance above chance (62.5% correct, with a 25% chance level), were determined using a cumulative Gaussian psychometric function.[96] Lower thresholds indicated better acuity. To convert Pelli digits' strokewidth to MAR, instead of taking 1/5 of the stimulus width as with the tumbling E, MAR was defined as 1/2 of the stimulus strokewidth.[12] Therefore, an optotype that was 2′ wide would correspond to the 20/20 Snellen MAR line. Individuals psychometric fits are shown in Figure S5.

Statistical analysis

Statistical comparisons were performed using a two-way repeated-measures analysis of variance (RANOVA) implemented in MATLAB R2022b (Mathworks, Natick, MA), with subject and condition treated as within-subject factors. The assumption of sphericity for repeated-measures factors was evaluated using Mauchly's test. In cases where sphericity was violated, *p*-values were corrected using the Greenhouse–Geisser method (p_{GG}), though this correction was not necessary for factors with only two levels. Following significant main effects or interactions, post hoc analyses were conducted using the Tukey–Kramer procedure to identify specific pairwise differences between conditions. Effect sizes for all reported effects were quantified using eta squared (η^2).

Pairwise comparisons

Planned pairwise comparisons between experimental conditions were conducted using paired two-tailed *t*-tests. To complement classical inference, Bayes factors (BF_{10}) were computed using the BayesFactor MATLAB toolbox (GitHub repository), providing a continuous measure of evidence for the alternative versus null hypothesis. Cohen's *d* was also calculated to quantify the magnitude of the observed effects.

Reporting summary

All statistical tests were two-tailed with a significance threshold of $\alpha = 0.05$. Data are reported as mean ± SEM unless otherwise stated. Statistical analyses were performed using custom scripts in MATLAB R2022b (MathWorks, Natick, MA).